High-flux two-dimensional magneto-optical-trap source for cold lithium atoms

T. G. Tiecke, S. D. Gensemer,* A. Ludewig, and J. T. M. Walraven
Van der Waals-Zeeman Institute, University of Amsterdam, Valckenierstraat 65, Amsterdam 1018 XE, The Netherlands
(Received 8 May 2009; published 20 July 2009)

We demonstrate a two-dimensional magneto-optical trap (2D MOT) as a beam source for cold ^{6}Li atoms. The source is side loaded from an oven operated at temperatures in the range $600 \lesssim T \lesssim 700$ K. The performance is analyzed by loading the atoms into a three-dimensional MOT located 220 mm downstream from the source. The maximum recapture rate of $\sim 10^9$ s^{-1} is obtained for $T \approx 700$ K and results in a total of up to 10^{10} trapped atoms. The recaptured fraction is estimated to be $30 \pm 10\%$ and limited by beam divergence. The most-probable velocity in the beam (α_z) is varied from 18 to 70 m/s by increasing the intensity of a push beam. The source is quite monochromatic with a full width at half maximum velocity spread of 11 m/s at $\alpha_z = 36$ m/s, demonstrating that side loading completely eliminates beam contamination by hot vapor from the oven. We identify depletion of the low-velocity tail of the oven flux as the limiting loss mechanism. Our approach is suitable for other atomic species.

DOI: 10.1103/PhysRevA.80.013409 PACS number(s): 37.10.−x, 37.20.+j, 34.50.−s

I. INTRODUCTION

Since the first demonstration of a laser-cooled atomic beam by Phillips and Metcalf [1] the development and improvement of cold atom sources has evolved into an essential activity in atomic physics laboratories. In particular sources for cold Rb, K, and Cs received a lot of attention and became compact and familiar standard devices [2]. However, for most other atomic and all molecular species the situation is less favorable and considerable time as well as resources remain necessary for the development of a source. Aside from optical cooling schemes many other cooling principles have been explored, we mention cryogenic cooling by surfaces [3] or buffer gas [4], filtering by magnetic [5,6] or electric funnels [7], and Stark deceleration of molecules [8] as well as Rydberg atoms [9]. In spite of the success of these sources in specific cases, optical cooling is the preferred option whenever an appropriate optical transition is available.

The highest optically cooled atom fluxes to date have been produced from Zeeman-slowed atomic beams [10–12,14]. Zeeman slowers have the additional advantage of a wide applicability. Unfortunately, their use adds a substantial engineering effort to system design and construction, in particular if beam-brightening and recycling principles are involved [11,15]. The magnetic field inside the Zeeman slower must be very smooth and satisfy a particular profile in order to optimize the slowing. In addition, as the acceptance angle is small, the source oven has to be positioned on the beam axis and operated under high flux conditions. In typical applications this gives rise to a high background of hot atoms and results in maintenance because the oven has to be reloaded regularly.

An important simplification of cold atom sources was realized when Monroe *et al.* [16] demonstrated that in a room-temperature vapor a fraction of the atoms can be optically captured and cooled into a magneto-optical trap (MOT) and subsequently loaded into a magnetic trap. The primary drawback of this vapor-cell MOT (VCMOT) is that the lifetime of the magnetically trapped atoms is limited by collisions with hot atoms from the vapor, thus limiting the time available for experiment. One approach to overcome this limitation is pulsed loading, starting from an alkali getter dispenser [17] or by ultraviolet light induced desorption [18,19]. All other solutions involve a dual chamber arrangement in which a source chamber, containing some variation of the VCMOT source, is separated by a differential pumping channel from an ultra-high-vacuum (UHV) chamber in which the atoms are recaptured in a secondary MOT in preparation for experiments under UHV conditions.

Three basic types of VCMOT sources are used in the dual MOT configurations. In the first type a pulsed VCMOT serves to load the recapture MOT by a sequence of cold atom bunches, transferred with the aid of a push beam [20]. The second type is known as the low-velocity intense source (LVIS) [21]. In this case the VCMOT and the push beam are operated continuously, giving rise to a steady beam of cold atoms in the direction of the push beam. In the third type the standard three-dimensional (3D) MOT arrangement in the source chamber is replaced by a two-dimensional (2D) MOT configuration, with (2D$^+$-MOT) or without (2D MOT) push and cooling beams along the symmetry axis [22–24]. This has the important advantage that the source MOT can be optimized for capture because, with confinement in only two directions, the residence time and collisional losses are intrinsically low.

VCMOT sources work most conveniently for elements such as Cs, Rb, and K, having a vapor pressure of $\sim 10^{-7}$ mbar around room temperature [25]. Elements such as Li, Yb, Cr, and the alkaline earths must be loaded from atomic beams since their vapor pressures are only significant at temperatures far above the maximum baking temperature of a conventional UHV system [12,25–28]. In the case of elements which are chemically reactive with glass, such as Li, a vapor cell is additionally impractical.

In this paper we present a 2D MOT source for cold lithium. It yields a cold flux comparable to the maximum achieved with lithium Zeeman slowers. Contrary to previ-

*Present address: Ethel Walker School, 230 Bushy Hill Rd, Simsbury, CT 06070, United States.

ously realized 2D MOT systems our source is transversely loaded with a beam from an effusive oven, rather than longitudinally like in beam brighteners or isotropically like in vapor cells. This demonstrates the possibility to use 2D MOT sources in applications where a vapor cell cannot be used and avoids the background of hot atoms in the beam. An important *a priori* uncertainty of this arrangement is the risk of depletion of the low-velocity tail of capturable atoms by the onset of nozzling as occurred in the famous Zacharias fountain experiment [29,30]. Our work shows that large cold atomic fluxes can be realized without this depletion becoming inhibitive. Recently this was also demonstrated with a Li oven loaded 3D MOT [31]. Another novelty of our source is the application of the 2D MOT concept to a light atom like lithium. Magneto-optical trapping of light species requires a high gradient for efficient capture. As this also compresses the cold atoms into a cloud of small volume, in particular in the 3D configuration trap losses are substantial even for small atom numbers. We demonstrate that in our dual MOT arrangement, the 2D MOT can be optimized for capture with a large gradient and without considerable losses, whereas the 3D recapture MOT can be optimized with a different gradient for maximum total atom number.

In the following sections we describe our experimental apparatus (Sec. II) and our results (Sec. IV). In Sec. III we present a simple model for the loading of the 2D MOT. The performance of our system and loss mechanisms are discussed in Sec. V and in Sec. VI we summarize our findings and comment on the suitability of our approach for other atomic species.

II. EXPERIMENT

A. Vacuum system

The experimental setup of the lithium 2D MOT source is sketched in Fig. 1. The vacuum system consists of a stainless steel six-way cross of 40 mm tubing of which two CF40 ports define the horizontal symmetry axis of the source. The other four CF40 ports are configured under 45° and sealed with standard vacuum windows providing the optical access for the retroreflected 2D MOT beams with a waist ($1/e^2$ radius) $w=9$ mm. A lithium oven is mounted with a CF16 flange onto the bottom of a water-cooled tube with inner radius $a=8$ mm and connected along the vertical axis into the center of the cross. The source is connected horizontally onto the main UHV chamber, separated by a gate valve. Between the main vacuum and the source a 23 mm long differential pumping (DP) channel of 2 mm diameter can maintain a maximum pressure ratio of 10^{-3} between the main UHV chamber and the source. There is no direct line of sight from the oven to the main UHV chamber nor to the windows. When the oven is operated and the 2D MOT lasers are off, no lithium was detected in the main UHV chamber. Also no measurable gas load is observed on the main vacuum while the source is operated.

B. Lithium oven

The oven consists of a stainless steel lithium reservoir, 25 mm high and 50 mm in diameter, attached to a CF16 flange

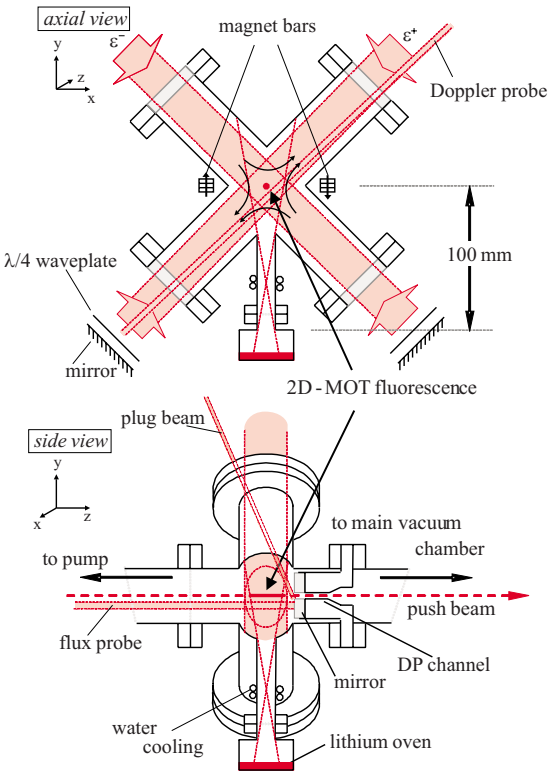

FIG. 1. (Color online) Schematic of the 2D-MOT system. The oven tube is welded into the center of a six way cross as described in the text. *Upper drawing*: vertical cross section through the oven viewing along the beam axis; *lower drawing*: vertical cross section through the oven and through the DP-channel viewing the beam from the side. The Doppler probe is under 50° with the vertical (y) axis and is used to calibrate the oven temperature. The flux probe is used to measure the hot flux emitted by the oven; a gold-plated mirror is included for this purpose. The plug beam is used to interrupt the atomic beam for time-of-flight measurements. The two-dimensional quadrupole field required for the 2D MOT is provided by two permanent-magnet bars.

by a 15 mm long tube of 16 mm inner diameter. The oven is embedded in a simple heat shield of glass wool and aluminum foil and is connected to the vacuum system using a nickel gasket. The reservoir was loaded with ~6 g of ^{6}Li and ~2 g of ^{7}Li under an inert gas (argon) atmosphere. As commercial lithium contains a large fraction of LiH it has to be degassed by dissociating the hydride. For this purpose we baked the oven under vacuum in a separate setup for 2 h at a temperature of ~943 K. Some 25% of the lithium was lost in this process. To protect the employed turbopump from alkali contamination a liquid nitrogen cold trap was used in this procedure.

Under typical conditions the oven is operated at $T=623(12)$ K (350 °C), well above the melting point of lithium at 454 K. All data presented in this paper, except those presented in Fig. 8, were obtained at this temperature. The oven temperature is calibrated by Doppler thermometry of the emerging Li flux using a probe beam under 50° with the vertical axis (see Fig. 1). Temperature stabilization is done with a thermocouple reference. Starting from room temperature the oven reaches the regulated value of 623 K in

~15 min. The ^{6}Li abundance was measured to be $a_6 = 0.74(5)$ using absorption spectroscopy on the ^{6}Li D_1 ($^2S_{1/2} \rightarrow {}^2P_{1/2}$) line and the ^{7}Li D_2 ($^2S_{1/2} \rightarrow {}^2P_{3/2}$) line.

C. 2D MOT configuration

As sketched in Fig. 1 the 2D MOT consists of a 2D quadrupole magnetic field in combination with two orthogonal pairs of retroreflected laser beams of opposite circular polarization, at a power of up to 50 mW per beam in a waist of 9 mm and red detuned with respect to the optical resonance near 671 nm. Like in a standard 3D MOT [2], a cold atom moving in the crossed laser field is optically pumped to a state for which the Zeeman shift places it closer to resonance with a laser opposing the motion of the atom. Thus the atoms are trapped and cooled in the radial direction and collect along the symmetry axis of the 2D quadrupole field but are free to move in the axial direction. As a result only atoms with a sufficiently low axial velocity can be radially trapped; atoms with a residence time of less then 0.5 ms in the optical trapping region leave the 2D MOT before they are significantly cooled. Only the radially cooled atoms give rise to a sufficiently collimated beam to pass through the DP channel and be recaptured by a 3D MOT in the middle of the UHV chamber.

For best performance the atoms are accelerated out of the source by a push beam, aligned along the symmetry axis and with a waist of 1.2 mm passing through the DP channel. The detuning and intensity of the push laser determine the velocity of the atoms emerging from the source. This velocity is chosen below the capture limit of the recapture MOT but is sufficiently fast to assure that the atoms do not fall below the recapture region as a result of gravity. For this reason the push beam is essential for horizontal configurations but optional in vertical arrangements. In all arrangements the push-beam acceleration increases the output flux because it reduces the residence time in the 2D MOT and therefore background-induced losses. In the literature on the $2D^+$ MOT [22–24] and the LVIS [21] control over the axial velocity is reported by using a pair of counterpropagating axial cooling beams over the entire trap but this method is not employed here.

The magnetic quadrupole field is provided by two sets of $Nd_2Fe_{14}B$ magnets (Eclipse magnets N750-RB) with a measured magnetization of $8.8(1) \times 10^5$ A m^{-1}. Each set consists of two stacks of three $25 \times 10 \times 3$ mm magnet bars separated by 12 mm to make an effective dipole bar of 62 mm total length. The optimum position of the centers of the dipole bars was experimentally found to be $x = \pm 42$ mm from the symmetry axis in the horizontal plane as sketched in Fig. 1. For this distance we calculate a field gradient of 0.50 T/m, constant within 2% along the 2D MOT symmetry axis over a total length of 20 mm. The use of permanent magnets simplifies the application of the high field gradients needed for light species. It combines a simple construction with convenient alignment and occupies much less space than the more traditional racetrack coils used by [22]. The quadrupole field falls off over short distances along the symmetry axis. At the position of the recapture MOT, 23 cm downstream from the center of the 2D MOT, only a small gradient of 210 μT/m remains.

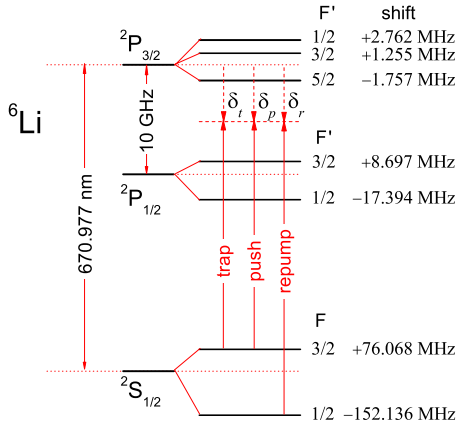

FIG. 2. (Color online) Level structure of ^{6}Li. Note that the hyperfine splitting of the $^2P_{3/2}$ levels is smaller than the natural linewidth $\Gamma/2\pi = 5.9$ MHz of the D_2 ($^2S_{1/2} \rightarrow {}^2P_{3/2}$) transition.

D. Hyperfine structure of ^{6}Li levels

Laser cooling of ^{6}Li, differs from the familiar case of ^{87}Rb, in which a spectrally well-resolved cycling transition on the D_2 line can be strongly driven to cool and trap the atoms while a weak repumping beam is sufficient to compensate for parasitic leakage to the dark state manifold. In the case of ^{6}Li the hyperfine splitting of the $2\,{}^2P_{3/2}$ excited state is of the order of the natural linewidth, $\Gamma/2\pi = 5.9$ MHz and all D_2 transitions from the $F=3/2$ manifold, $|2\,{}^2S_{1/2}; F=3/2\rangle \rightarrow |2\,{}^2P_{3/2}; F'=1/2,3/2,5/2\rangle$ are excited simultaneously (see Fig. 2) [32]. Hence, there is no closed transition suitable for cooling and trapping and strong optical pumping to the $|2\,{}^2S_{1/2}; F=1/2\rangle$ level cannot be avoided. As a consequence the "trapping" and "repumping" beams have to be of comparable intensities, which means that both beams contribute to the cooling and mutually serve for repumping. Also the detunings will have a strong influence in this respect [33]. In spite of these differences we stick to the conventional terminology, referring to the transition $|^2S_{1/2}; F=3/2\rangle \rightarrow |^2P_{3/2}; F'=1/2,3/2,5/2\rangle$ as the trapping transition and to $|^2S_{1/2}; F=1/2\rangle \rightarrow |^2P_{3/2}; F'=1/2,3/2\rangle$ as the repumping transition.

E. Laser system

A laser system for wavelength $\lambda_L = 671$ nm was developed to serve the 2D (source) MOT and the 3D (recapture) MOT as well as to provide laser beams for ^{6}Li diagnostics. The laser system consists of a single master oscillator and four injection-locked slave lasers, all operating a 120 mW Mitshubishi ML101J27 diode heated to 70 °C. The master oscillator is a home-built external-cavity diode laser (ECDL) [34], frequency stabilized using saturated absorption spectroscopy in a ^{6}Li heat pipe [35]. The power from the master laser is distributed over six beams, which can be independently shifted in frequency using ISOMET 1205-C acousto-optic modulators (AOM's). Of these six beams four are am-

plified by injection locking of the slave lasers and of these four beams one pair is used for the retroreflected trapping and repumping beams of the 2D MOT while the other pair is equally distributed over six beams and similarly employed for the 3D MOT. The remaining two frequency-shifted ECDL beams serve as pushing beam, as probing beam or as plug beam in various diagnostic applications.

III. SOURCE MODEL

A. Oven flux

To establish the principle of our source and to enable comparison with experiment we present a semiempirical kinetic model in which the oven is replaced by an emittance of area $A=\pi a^2\approx 2$ cm^2 at the saturated vapor pressure of lithium. Around $T=623$ K the saturated vapor pressure is given by $p_s=p_a \exp(-L_0/k_BT)$ where $p_a=1.15(5)\times 10^{10}$ Pa and $L_0/k_B=18474$ K is the latent heat of vaporization [25]. As p_s is only accurate to within 5% we neglect the small dependence on the isotopic composition. The total atomic flux Φ_{tot} emitted by the oven may be estimated by the detailed balance expression for the total flux onto and from the emittance under thermal equilibrium conditions,

$$\Phi_{tot}=\frac{1}{4}n_s\bar{v}A, \tag{1}$$

where n_s is the atomic density and $\bar{v}=[8k_BT/\pi m]^{1/2}$ the mean thermal speed, with k_B the Boltzmann constant and m the mass of the Li atoms. For $T=623(12)$ K we have $p_s=1.5^{+1.1}_{-0.7}\times 10^{-3}$ Pa, corresponding to a density $n_s=1.8^{+1.2}_{-0.8}\times 10^{17}$ m^{-3}. With these numbers the total flux from the source is found to be $\Phi_{tot}\approx 1.3\times 10^{16}$ s$^{-1}\approx 1.3\times 10^{-10}$ kg s^{-1}. With 8 g of Li this corresponds to $\sim$17 000 h running time.

The flux of ^{6}Li atoms captured by a 2D MOT at a distance of $L=100$ mm above the oven can be written as an integral over the velocity distribution

$$\Phi_c=a_6n_sA\int_0^{\Omega_c}d\Omega\frac{\cos\theta}{4\pi}\frac{1}{\mathcal{N}}\int_0^{v_c}v^3e^{-(v/\alpha)^2}dv, \tag{2}$$

where $a_6=0.74(5)$ is the ^{6}Li abundance, $\Omega_c=A_c/L^2=2\times 10^{-2}$ the solid angle of capture (with A_c the capture surface), $d\Omega=2\pi\sin\theta d\theta$ with θ the emission angle with respect to the oven axis, v_c the capture velocity, $\alpha=[2k_BT_0/m]^{1/2}=1.31\times 10^3$ m/s the most-probable atomic speed in the oven and $\mathcal{N}=\int v^2e^{-(v/\alpha)^2}dv=\pi^{1/2}\alpha^3/4$ the normalization factor of the speed distribution. Note that by integrating Eq. (2) over a hemisphere we regain Eq. (1) in the limit ($a_6\to 1; v_c\to\infty$). Because the solid angle of capture is small we have $\cos\theta\simeq 1$ and the flux Φ_s emitted by the oven within the solid angle of capture is given by

$$\Phi_s\simeq n_s\bar{v}A\frac{\Omega_c}{4\pi}. \tag{3}$$

For $T=623(12)$ K we calculate a total flux density of $\Phi_s/A_c=4^{+3.2}_{-1.6}\times 10^{13}$ s^{-1} cm^{-2} at $L=100$ mm above the oven. Presuming the capture speed to be small, $v_c\ll\alpha$, the captured flux Φ_c may be approximated by

$$\Phi_c\simeq\frac{1}{2}a_6n_s\bar{v}A\left(\frac{v_c}{\alpha}\right)^4\frac{\Omega_c}{4\pi}=\frac{1}{2}a_6\left(\frac{v_c}{\alpha}\right)^4\Phi_s. \tag{4}$$

This expression represents the theoretical maximum flux that can be extracted from the 2D MOT source.

B. Capture and cooling

To discuss the capture and cooling behavior in the 2D MOT we distinguish two coaxial spatial regions, crossing-over at $r=r_d$ defined by $\delta_Z(r_d)+\delta_L=0$, i.e., the surface where the Zeeman shift in the radial gradient of the quadrupole field, $\hbar\delta_Z(r)=\mu_B(\partial B/\partial r)r$, is compensated by the detuning of the laser, $\delta_L=\omega_L-\omega_0<0$, i.e., to the red side of the cooling transition at angular frequency ω_0 in zero field.

In the outer region ($r>r_d$), the 2D MOT functions much like a Zeeman slower, while in the inner region ($r<r_d$) the motion of the atoms can be described by a damped harmonic oscillator model [2]. First we discuss the outer region. An atom with velocity $\mathbf{v}$ at distance r from the symmetry axis will be at resonance with the cooling laser if the difference of the Zeeman shift and the laser detuning equals the Doppler shift,

$$\delta_Z-\delta_L=-\mathbf{k}\cdot\mathbf{v}. \tag{5}$$

Here $k=|\mathbf{k}|=2\pi/\lambda_L$ is the wavevector of the cooling laser. In view of the angle of 135° between the directions of the hot lithium beam and the opposing laser cooling beams the positive Doppler shift is reduced by a factor $-\cos(\mathbf{k},\mathbf{v})=\sqrt{1/2}$ with respect to the fully counterpropagating configuration. Accordingly, the maximum available slowing distance is larger, $r_{\max}=\sqrt{2}w$, where $w=9$ mm is the waist of the cooling beams. Substituting $r_{\max}$ in the expression for the Zeeman shift we rewrite Eq. (5) in the form of an expression for the highest atomic speed $v_{\max}$ for which the resonance condition is satisfied

$$v_{\max}=\lambda_L\frac{\sqrt{2}}{2\pi}\left[\frac{\mu_B}{\hbar}\frac{\partial B}{\partial r}r_{\max}-\delta_L\right]. \tag{6}$$

Note that with the left-circular (ϵ^+) and right-circular (ϵ^-) polarizations of the 2D MOT beams as indicated in Fig. 1 the atoms are σ^+ optically pumped into a fully stretched state with the magnetic field being orthogonal to the propagation direction of the hot flux. In the simplest 1D model for capture process (in which only the trajectory along the symmetry axis of the oven is considered) $r_{\max}$ represents the capture radius (r_c) and $v_{\max}$ the capture velocity (v_c) of the 2D MOT provided the resonant photon scattering force ($mdv/dt=\hbar k\Gamma/2$) is large enough to keep the atom in resonance with the cooling laser, $\hbar d\delta_Z/dt=-\mu_B(\partial B/\partial r)v_{\max}$. The resulting condition

$$v_{\max}\le\frac{\sqrt{1/8}(\hbar k)^2}{m\mu_B(\partial B/\partial r)}\Gamma \tag{7}$$

is satisfied in our experiment. Combining Eqs. (6) and (7) we obtain an equation quadratic in $(\partial B/\partial r)$, which reduces for $\delta_Z\gg\delta_L$ to

$$\frac{\partial B}{\partial r} \leq \frac{(\hbar k)^{3/2}}{2\mu_B (m r_{\max})^{1/2}} \Gamma^{1/2}. \tag{8}$$

This expression shows that the optimal gradient for capture scales like $m^{-1/2}$, which is important for comparing the performance of the source for different atomic species. Substituting the optimal gradient into Eq. (7) we obtain

$$v_{\max} = (a_{\max} r_{\max})^{1/2}, \tag{9}$$

where $a_{\max} = \hbar k \Gamma / 2m$ is the maximum attainable deceleration by the scattering force.

In spite of the insight it offers the 1D model is far too simple to justify the use $v_c = v_{\max}$ for reliable estimates of the captured flux. Therefore, we decided to estimate v_c experimentally by measuring the loading rate of the 3D MOT as a function of the mean velocity in the cold beam and Eq. (6) is only used for scaling between the conditions of the 3D MOT and the 2D MOT. This procedure is discussed in Sec. V.

In the inner region ($r < r_d$) of the trap the atomic motion is described by an overdamped harmonic oscillator model with a spring constant κ and damping coefficient β [2]. The atoms approach the axis with the cooling time constant $\tau \simeq \beta / \kappa$. For our 2D MOT parameters $\tau \approx 0.5$ ms. Atoms entering the 2D MOT with velocity $v < v_c$ only contribute to the cold lithium beam if τ is less than the residence time τ_{res} in the trapping beams ($\tau < \tau_{\text{res}}$). In the absence of collisions with background gas τ_{res} is determined by the velocity component $|v_z| \lesssim v_c a / L$ of the trapable lithium atoms along the symmetry axis of the 2D MOT and the entry point in the optical field. If even the atoms with the shortest residence time can still be cooled, i.e., for

$$|v_c| \lesssim \frac{w}{a} \frac{L}{\tau + \tau_Z} \simeq \frac{L}{\tau} \tag{10}$$

essentially all captured atoms contribute to the cold beam. For $L = 100$ mm we calculate with $\tau = 1$ ms that this condition is satisfied for $v_c \lesssim 100$ m/s, including the experimental value $v_c \approx 85$ m/s (see Sec. V).

IV. EXPERIMENTAL RESULTS

A. Oven flux

To evaluate the merits of the 2D MOT it is essential to have a reliable estimate of the input flux from the lithium oven. For this purpose the oven flux was measured at $T = 623$ K by observing—in the absence of the $Nd_2Fe_{14}B$ magnets—the Doppler profile of the hot lithium beam using a horizontal probe beam with a waist of 1 mm running parallel to the 2D MOT axis and back reflected by a gold-plated mirror (spring mounted at the entrance of the DP-channel) as indicated in Fig. 1. To avoid optical pumping to dark states the probe intensity was kept at the low value of $\sim 0.018 I_{sat}$. With a thermal velocity of $\bar{v}_{th} = 1500$ m/s the interaction time is 1.3 μs and the scattering rate is estimated to be 0.4 photons per atom. The effect of small fluctuations in the intensity of the probe laser was suppressed by measuring the intensity of the probe beam relative to that of a reference beam originating from the same laser diode. Both the probe beam and the reference beam were measured with Texas Instruments OPT101 photodiodes. The observed Doppler profile is shown in Fig. 3. The solid line represents a fit of the calculated Doppler profile for the oven temperature $T = 623$ K and presuming the measured ^{6}Li abundance. The solid line is the sum of six overlapping Doppler broadened lines (dotted lines). The unusual lineshapes reflect the clipping profile of the oven tube. The two large peaks at 0 and 228 MHz correspond to the trapping and repumping transitions in ^{6}Li, respectively. Analogously the other four peaks at 199, 291, 1002, and 1094 MHz are for the $F = 2 \rightarrow F' = 1, 2$ and $F = 1 \rightarrow F' = 1, 2$ transitions of the D_1 line of ^{7}Li [32]. The best fit is obtained for $\Phi_s = 8(3) \times 10^{13}$ s^{-1}, where the error reflects our estimate of systematic uncertainties. This result overlaps with the value $\Phi_s = 8^{+6.4}_{-3.2} \times 10^{13}$ s^{-1} calculated with Eq. (3) of the semiempirical model starting from the oven temperature.

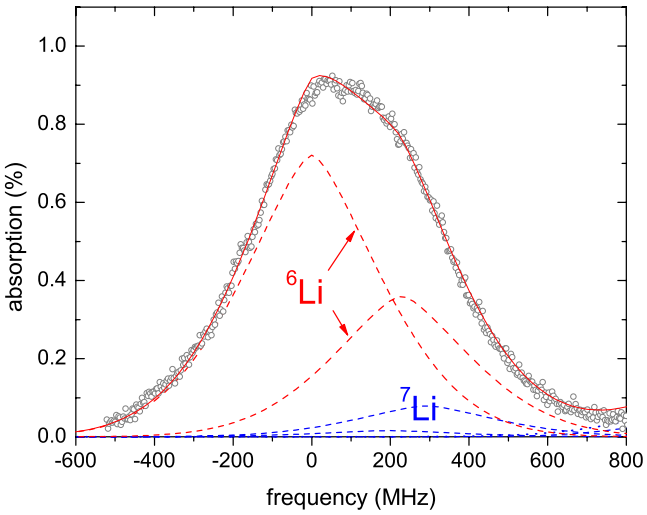

FIG. 3. (Color online) The transverse Doppler profile of the hot lithium flux emerging from the oven as measured with the horizontal probe beam indicated in Fig. 1. The calculated profile (solid line) is the sum of six overlapping Doppler broadened transitions (dotted lines), two of which have a maximum outside the frequency range shown (see text). Only the amplitude has been fitted presuming the measured oven temperature $T = 623$ K and ^{6}Li abundance of 74%.

B. Fluorescence detection: TOF distribution

We probe the intensity of the cold ^{6}Li beam in the middle of the main vacuum chamber by measuring the fluorescence after flashing a sheet of resonant laser light (knife-edge defined: $d = 1$ mm thick and $h = 5$ mm high) propagating horizontally through the middle of the UHV chamber orthogonal to the beam axis at position $z = L_a = 220$ mm downstream from the entry point of the DP channel. The fluorescence flash is imaged vertically as a stripe onto a charge-coupled device (CCD) camera. The length of the stripe provides information about the divergence of the beam. To remove stray-light fluctuations the integrated signal from the pixel area containing the stripe image is divided by the background signal from a reference area. For the probe beam we use 0.5 ms flashes of 0.3 W cm^{-2} in a ratio of 1:1.5 trap/

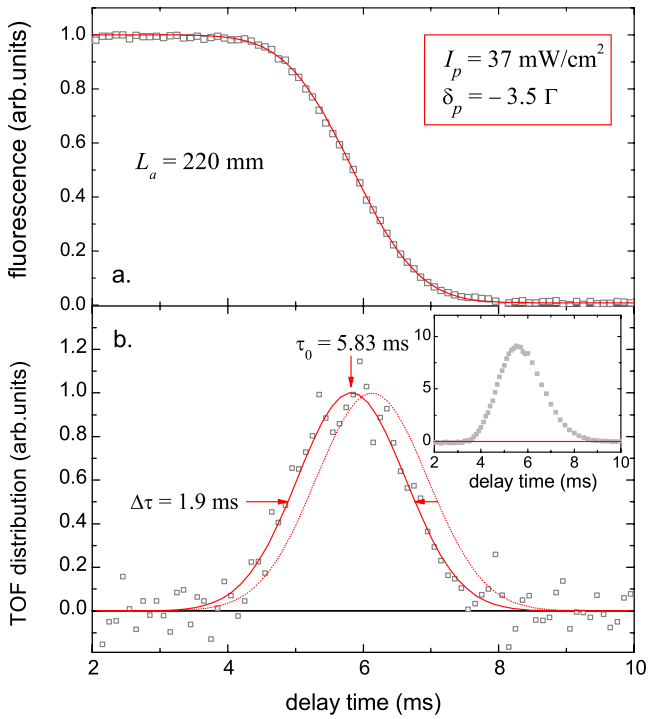

FIG. 4. (Color online) (a) Typical fluorescence decay curve as a function of the probe delay time. The solid line is a fitted error function. Each data point represents the average over 200 cycles taken over a period of 6.7 s. (b) Derivative of the same data. The dashed line represents the true TOF distribution (normalized to the same peak height) as calculated with the model presented in the text. The inset shows a TOF distribution as measured with a pulsed push beam.

repump light at zero detuning. The beam is retroreflected to prevent the atoms from being pushed out of resonance.

Velocity characterization of the cold ^{6}Li beam is done with a time-of-flight (TOF) method. For this purpose the beam is periodically interrupted at typically 30 Hz repetition rate with a resonant 0.6 W cm^{-2} "plug" laser (2:1 trap:repump light) deflecting the atoms near the entrance of the DP channel. From the decay of the fluorescence signal $\phi_{\rm fl}$ as a function time (see Fig. 4) we obtain the apparent TOF distribution, which is proportional to $d\phi_{\rm fl}/d\tau$ and can be transformed into the axial velocity distribution using the flight distance of 220 mm. In a typical measurement we average over 200 cycles to reach a proper signal/noise ratio also for small fluxes traversing the light sheet at high velocity.

The procedure is illustrated in Fig. 4 for a push-beam intensity of I_p=37 mW cm^{-2} and a detuning δ_p=−3.5Γ. Note that the derivative of $\phi_{\rm fl}$ can be nicely described by the Gaussian function

$$d\phi_{\rm fl}/d\tau = (\pi^{1/2}\Delta\tau)^{-1}\exp[-(\tau-\tau_0)^2/\Delta\tau^2], \qquad (11)$$

where τ_0=5.83 ms is the mean apparent arrival time and $1.67\Delta\tau$=1.9 ms is the full width at half maximum (FWHM). The absence of arrival times shorter than 3 ms reflects the absence of atoms with velocities $v_z \gtrsim 70$ m/s. This absence of "hot" flux was verified up to 4 km/s and was anticipated because the cold beam is pushed horizontally out of the 2D MOT, i.e., orthogonally to the hot flux from the oven. The observed relative spread $\Delta\tau/\tau_0 \approx 0.2$ is insensitive to the push-beam intensity and comparable to the instrumental resolution for the shortest flight times investigated (τ_0=3 ms). The value of τ_0 is entirely determined by the properties of the push beam and insensitive to other 2D MOT parameters. This behavior was previously also observed in other 2D MOT systems [23,24]. Since optical pumping to different hyperfine states takes only a few optical cycles in ^{6}Li and L_a/τ_0=38 m/s corresponds to ~380 photon recoils, the atoms must have been accelerated to their final velocity still within reach of the repump light, i.e., inside 2D MOT (the push beam does not contain repumper light). This limits the acceleration to a well-defined duration of time, which is consistent with the observed relatively narrow velocity distribution. The absence of slow atoms is not caused by gravity because for the lowest velocities measured (L_a/τ_0 =22 m/s) the gravitational drop is only 0.5 mm, less than half the height ($h/2$=2.5 mm) of the light sheet.

To relate the fluorescence signal $\phi_{\rm fl}$ to the velocity distribution in the atomic beam we have to account for the detection efficiency, which is inversely proportional to the velocity of the atoms and depends on the divergence of the beam. For this purpose we approximate the beam spot at the position of the light sheet ($z=L_a$) by a Gaussian profile with $1/e$-radius R. The fraction $\chi_{\rm fl}$ of the beam giving rise to fluorescence is obtained by integrating the normalized Gaussian beam profile in horizontal and vertical direction over the surface area of the light sheet,

$$\chi_{\rm fl} = \mathrm{erf}(h/2R)\mathrm{erf}(S_0/R), \qquad (12)$$

where S_0=4.5 mm is the radius of the optical field of view. Here we neglected some clipping by the DP channel. Note that the divergence angle ζ of the cold beam equals the ratio of transverse to axial velocity of the atoms, $\zeta = R/L_a = v_t/v_z$. The length of the fluorescence stripe was found to vary only slightly with the intensity of the push beam. This sets a lower bound on the beam divergence, $S_0/R \lesssim 1$ for v_z=70 m/s and on the characteristic transverse velocity, $v_t \gtrsim 1.4$ m/s. Since $h/2R \ll S_0/R \lesssim 1$ for all velocities studied Eq. (12) can be written in the form

$$\chi_{\rm fl}(v_z/v_t) \simeq \gamma v_z/v_t\ \mathrm{erf}(\eta v_z/v_t), \qquad (13)$$

where $\eta = S_0/L_a$=0.02 is the view angle and $\gamma = h/2L_a$ =0.011 the vertical acceptance angle.

The fluorescence decay signal $\phi_{\rm fl}$ can be expressed in the form

$$\phi_{\rm fl}(\tau) \sim \int_0^{L_a/\tau} \frac{\chi_{\rm fl}(v_z/v_t)}{v_z}\phi_0(v_z,\alpha_z)dv_z, \qquad (14)$$

where $\phi_0(v_z,\alpha_z)$ is the normalized axial velocity distribution with α_z representing the most-probable velocity in the beam, and L_a/τ the velocity of the fastest atoms still arriving at the detector after delay time τ. Hence, the transformation between the beam property $\phi_0(v_z,\alpha_z)$ and the observed fluorescence decay is given by

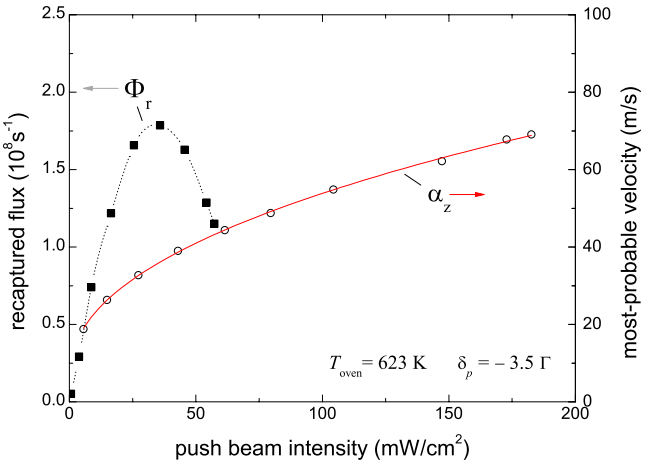

FIG. 5. (Color online) Recapture rate into the 3D MOT (solid squares—left scale) and the most-probable axial velocity (α_z) of the cold atomic beam (open circles—right scale) both as a function of the push-beam intensity. The drawn lines provide a guide to the eyes.

$$\phi_{\mathrm{TOF}}(\tau) = \phi_0(L_a/\tau) \propto -(\tau/\chi_{\mathrm{fl}})d\phi_{\mathrm{fl}}/d\tau. \tag{15}$$

Here $\phi_{\mathrm{TOF}}(\tau)$ represents the distribution of flight times in the beam. For $\Delta\tau/\tau \ll 1$ the prefactor $(\tau/\chi_{\mathrm{fl}})$ causes the distribution $d\phi_{\mathrm{fl}}/d\tau$ to shift to larger delay times but its shape remains well described by a Gaussian. In our case the shift is 5% ($\tau_{\max} \simeq 1.05\tau_0$) as indicated by the dotted line in Fig. 4. Hence, the most-probable velocity in the beam is given by $\alpha_z \simeq 0.95 L_a/\tau_0$. For the example of Fig. 4 we calculate $\alpha_z = 36$ m/s with a FWHM of 11 m/s. We have observed a tenfold increase in $\phi_{\mathrm{TOF}}(\tau)$ at constant average flux by pulsing the push beam (see inset in Fig. 4). This indicates that the 2D MOT is not limited by its density when the push beam is continuously on. The most-probable velocity α_z was found to be the same for pulsed and continuous operation. The experimental results for α_z as a function of the push-beam intensity are shown as the open circles in Fig. 5. Varying the push-beam intensity I_p over the range 5–180 mW cm^{-2} we found α_z to increase from 18–70 m/s.

C. Beam flux: Dependence on the push beam

The flux of the cold atomic beam is investigated as a function of the push-beam intensity (I_p) by recapture into the 3D MOT. The results are shown as the solid squares in Fig. 5. First of all we note that in the absence of the push beam the flux arriving at the recapture MOT is very small. Under these conditions the 2D MOT performance is very sensitive to the alignment of the quadrupole field, the MOT beams, and the repumper. This low flux is attributed to the horizontal orientation of the beam axis, orthogonal to the direction of the hot flux from the oven. In view of this symmetry the trapped atoms have an axial velocity distribution centered around zero. Only the atoms with axial velocity $v_z \gtrsim 5$ m/s will reach the capture volume of the 3D MOT. Slower atoms drop below the trapping region as a result of gravity. High-field-seeking atoms will be deflected away from the recapture MOT by the quadrupole field outside the 2D MOT for axial velocities $v_z \lesssim 10$ m/s. Atoms with axial velocity $v_z \gtrsim 0.1\, v_c \approx 8.5$ m/s are absent due to clipping by the oven tube (v_c is the capture velocity of the 2D MOT).

As an aside we point out that by inclining the axis of the oven tube toward the beam axis direction it should be possible to realize a high flux cold beam with an axial velocity proportional to the inclination angle and without any (near) resonant light copropagating with the atomic beam into the UHV chamber. In a more practical solution this may be realized by not retroreflecting the 2D-MOT beams but tilting them so that the average **k**-vector points along the cold beam axis.

Measuring the loading rate Φ_r in the 3D MOT we obtain the "useful" flux of the cold ^{6}Li beam. The rate is obtained from the leading slope of the loading curve, observing the 3D MOT fluorescence as a function of time using a CCD camera. This fluorescence is calibrated against an absorption image taken immediately after switching off the 3D MOT. The measured rate Φ_r represents a lower limit for the flux emerging from the 2D MOT. Figure 5 shows that Φ_r increases steeply until it reaches a maximum at $I_p \approx 34$ mW cm^{-2}. Further increase of the push-beam intensity causes the loading rate to decrease. This is attributed to the finite capture velocity of the 3D MOT (see Sec. V). For the data shown in Fig. 5 we used for the 3D MOT a magnetic field gradient of 0.19 T/m, 10 mW trapping light per beam at a detuning of −6 Γ and 11 mW repumping light per beam at a detuning of −3.5 Γ. Both colors are distributed over six beams clipped at their beam waist of 9 mm, thus defining the acceptance radius $R_a = 9$ mm of the 3D MOT.

D. Beam flux: Dependence on the 2D MOT

We have optimized the total flux by varying both the trap and the repump detuning. For these measurements the laser power of the trap and repump lasers were set to their maximum values of 100 and 94 mW, respectively. The results are shown as a contour diagram in Fig. 6. The maximum flux is observed when the trap laser is far detuned ($\delta_t = -7.5\Gamma$) and the repump laser is close to resonance ($\delta_r = -1\Gamma$). We observe a small local maximum in flux if the trap laser is tuned close to resonance ($\delta_t = -1\Gamma$). We attribute this to better beam collimation because the 2D MOT is expected to be transversely colder when operated close to resonance [36,33]. Apparently the advantage of better collimation cannot compensate loss in 2D MOT capture efficiency.

With optimized detunings we measured Φ_r as a function of the available optical power in the 2D MOT trap (P_t) and repump (P_r) beams. For this purpose either the trapping power is kept constant at $P_t \approx 50$ mW per beam and P_r is varied or the repumping power is kept constant at $P_r \approx 48$ mW per beam and P_t is varied. As is shown in Fig. 7 the loading rate increases linearly with P_t for $P_t \gtrsim 8$ mW, whereas Φ_r increases linearly with P_r for $P_r \gtrsim 2$ mW until it levels off for $P_r \gtrsim 18$ mW. The experimental parameters for optimal source performance are collected in Table I. The output flux was reproducible to within 30% depending on the 2D MOT alignment.

E. Beam flux: Dependence on the oven temperature

Figure 8 shows the loading rate as a function of the oven temperature. At low temperatures the loading rate increases

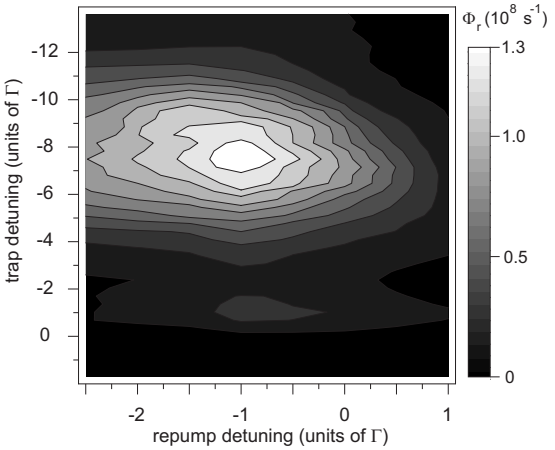

FIG. 6. The 3D MOT loading rate as a function of the 2D MOT trap and repump detunings for an oven temperature $T=623(12)$ K. These measurements were performed with maximum power for the 2D MOT trap and repump beams as given in Table I. We find the maximum flux of 1.3×10^8 s^{-1} at a trap detuning of $\delta_t=-7.5\Gamma$ and $\delta_r=-1\Gamma$.

exponentially with the oven temperature. This reflects the exponential increase of the effusive flux from the oven. Above $T\approx650$ K a loss mechanism sets in. This limits further increase of the flux until at $T\approx700$ K the cold atomic flux reaches its maximum value, corresponding to a loading rate of $\Phi_r=8(3)\times10^8$ s^{-1} into the 3D MOT. The error reflects our best estimate of systematic uncertainties. As will be will be discussed in Sec. V the losses are attributed to knock-out collisions in the effusive beam emerging from the oven. The dotted line shows the fraction of atoms surviving the loss mechanism.

V. DISCUSSION

A. Recapture in the 3D MOT

To analyze the performance of the 2D MOT source we define the overall efficiency parameter χ as the ratio of the

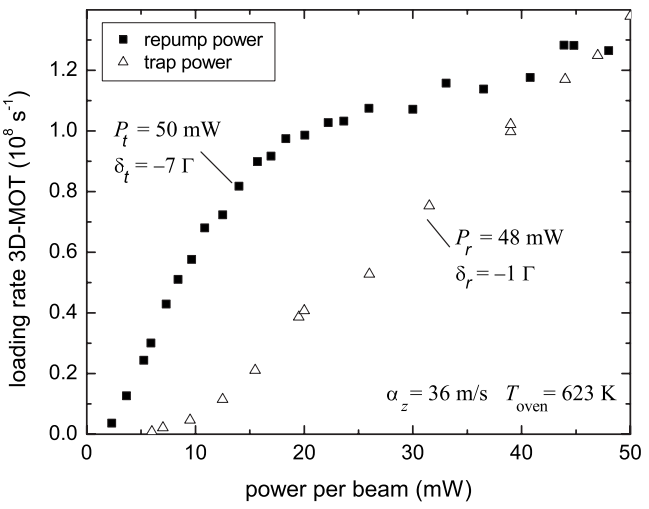

FIG. 7. The 3D MOT loading rate as a function of the 2D trap and 2D repump laser powers (power per beam). Note that the 2D MOT is operated in a retroreflected configuration.

TABLE I. Experimental parameters for optimal performance of the Li 2D MOT.

Parameter	Trap	Repump	Push
Detuning δ	$-7.5\ \Gamma$	$-1\ \Gamma$	$-3.5\ \Gamma$
Power per beam	50 mW	48 mW	0.8 mW
Waist ($1/e^2$ radius)	9	9	1.2
Gradient	0.5 T/m		
Oven temperature	623 K		
Most-probable velocity	36 m/s		
FWHM of velocity distribution	11 m/s		

3D MOT loading rate Φ_r and the maximum capturable flux Φ_c from the oven,

$$\Phi_r=\chi\Phi_c.$$

This efficiency is determined by the capture efficiencies of the 2D and 3D MOT as well as the transfer efficiency χ_t related to the divergence of the atomic beam. To determine χ_t as well as the capture velocity v_c we replotted the data of Fig. 5 in the form of Fig. 9, showing the capture rate Φ_r in the 3D MOT as a function of the most-probable axial velocity α_z in the cold atomic beam. Like in Sec. IV B we approximate the atomic beam profile at the position of the 3D MOT ($z=L_a=220$ mm) by the Gaussian profile with $1/e$-radius R. The transfer efficiency is obtained by integrating the normalized profile from $r=0$ on the beam axis to the acceptance radius $r=R_a=9$ mm of the 3D MOT,

$$\chi_t(x_a)\simeq 2\int_0^{x_a}(1-x/x_0)e^{-x^2}xdx. \tag{16}$$

Here $x=r/R$, $x_a=R_a/R$, and $x_0=R_0/R$. The factor $(1-x/x_0)$ represents the conical approximation to the trapezoidal clip-

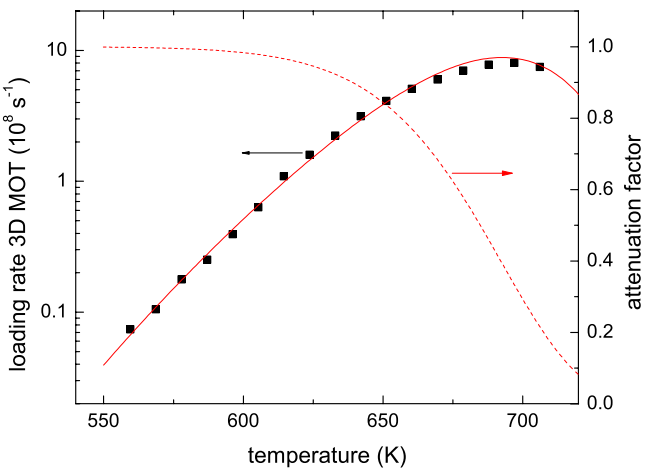

FIG. 8. (Color online) The 3D MOT loading rate as a function of oven temperature (solid squares—left scale). The solid line shows a fit of the model presented in Sec. V. The loading rate reaches a maximum of 8×10^8 s^{-1} at $T\approx700$ K as a result of beam attenuation by hot background vapor. The calculated attenuation factor is shown as the dashed line (right scale).

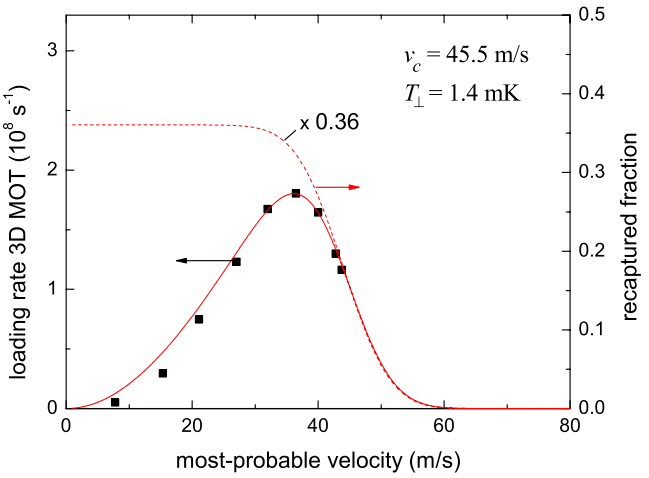

FIG. 9. (Color online) Loading rate 3D MOT as a function of the most-probable velocity α_z in the beam (black squares—left scale). The drawn line represents the best fit to the data of the recapture model described in the text for v_c=45.5 m/s (right scale). The result for zero beam divergence is shown as the dotted line, scaled down with a factor 0.36 for convenience of comparison.

ping profile imposed by the DP channel, where R_0=19 mm marks the edge of the dark shadow. Defining the 3D MOT acceptance angle $\alpha=R_a/L_a$ and velocity ratio $\tilde{v}_z \equiv v_z/v_t = 1/\zeta$ we write compactly $x_a=\alpha\tilde{v}_z$. Similarly we define the clipping angle $\beta=R_0/L_a$ and write $x_0=\beta\tilde{v}_z$. Substituting the expressions for x_a and x_0 into Eq. (16) and evaluating the integral we obtain for the transfer efficiency

$$\chi_t(\tilde{v}_z) = 1 - (1-\alpha/\beta)e^{-(\alpha\tilde{v}_z)^2} - \frac{1}{2\beta\tilde{v}_z}\sqrt{\pi}\,\mathrm{erf}(\alpha\tilde{v}_z). \quad (17)$$

The velocity-averaged transfer efficiency (recaptured fraction) into the 3D MOT is given by

$$\bar{\chi}_t(\alpha_z, v_c) = \int_0^{v_c} \chi_t(v_z/v_t)\phi_0(v_z,\alpha_z)dv_z, \quad (18)$$

where $\phi_0(v_z,\alpha_z)$ is the normalized axial velocity distribution defined by Eq. (15). The solid line in Fig. 9 is a plot of $\bar{\chi}_t(\alpha_z,v_c)$ for a fixed value of v_c. The position of the maximum is insensitive for the beam divergence and the best fit is obtained for a capture velocity of v_c=45.5 m/s. In contrast the peak height $\bar{\chi}_{\max}$ depends strongly on the beam divergence. Using the lower limit for the characteristic transverse velocity ($v_t \gtrsim 1.4$ m/s) we calculate an upper limit for the recaptured fraction $\bar{\chi}_{\max} \lesssim 0.4$. For comparison also the result for zero beam divergence is shown in the plot (dotted line).

For the conditions used in experiment, $\partial B/\partial r$ =0.19 T/m and $\delta_L=-6\Gamma$, we calculate with Eq. (6) $v_c=32+5.6|\delta_L/\Gamma| \approx 66$ m/s for $r_c=\sqrt{2}R_a=12.7$ mm. Apparently the simple one-dimensional model overestimates the capture velocity by some 50%. Because both the 2D MOT and the 3D MOT are configured in the 135° configuration with respect to the input beam and also r_c=12.7 mm in both cases we presume a similar overestimate for the capture velocity of the 2D MOT. In the latter case we have $\partial B/\partial r$=0.50 T/m and $\delta_L=-7.5\Gamma$ and calculate with Eq. (6) $v_c=85+5.6|\delta_L/\Gamma| \approx 127$ m/s. Presuming somewhat arbitrarily that also this value overestimates the actual capture velocity by 50% we obtain $v_c \approx 85$ m/s as a reasonable estimate.

Starting from $\Phi_s=8(3)\times10^{13}$ s^{-1} we obtain with Eq. (4) for the theoretical maximum flux $\Phi_c=5(2)\times10^8$ s^{-1}. With the measured value $\Phi_r=1.8(6)\times10^8$ s^{-1} the overall efficiency $\chi=\Phi_r/\Phi_c$ is estimated to be $0.2 \lesssim \chi \lesssim 0.5$. This set a lower limit on the recaptured fraction, $0.2 \lesssim \bar{\chi}_{\max} \lesssim 0.4$, and (using our model) also an upper limit for the characteristic transverse velocity, $v_t \lesssim 2.5$ m/s. As the upper and lower limits more or less coincide our best estimate is $v_t \approx 2$ m/s, which corresponds to a transverse 2D MOT temperature of $T_\perp$=1.4 mK. The corresponding beam divergence at optimal recapture for oven temperature T=623(12) K is $\zeta \approx 0.05$. For these conditions the brightness of the beam emerging from the 2D MOT is calculated to be $\sim 2\times10^{11}$ sr^{-1} s^{-1}.

B. Loss mechanisms

Because $\Phi_c \ll \Phi_s$ the output from the oven is well characterized by a small cold flux of capturable atoms overtaken by the hot flux of the full emittance. Once the hot flux exceeds a critical value we expect the cold flux to be attenuated by "knock-out" collisions. This depletion of the low velocity class of atoms is a well-known phenomenon in close-to-effusive beam sources [29]. Comparing the total flux per unit area just above the emitting surface, $\Phi_{tot}/A \approx 6.5\times10^{15}$ s^{-1} cm^{-2}, with the flux per unit area in the capture region $\Phi_s/A \approx 4\times10^{13}$ s^{-1} cm^{-2}, we expect these knock-out collisions to occur primarily in the first few centimeters of the expanding beam. Once the atoms enter the 2D MOT the cross section increases because optically excited atoms interact resonantly with the hot background flux [40].

To model the attenuation we calculate the collision rate of an atom moving at velocity v_c along the symmetry axis at position l above the oven exit orifice with atoms from the hot background flux moving at typically the average velocity $\bar{v} \gg v_c$,

$$\dot{\Phi}/\Phi = \frac{1}{2}\sigma_6 n_s \int_0^{\theta_0(l)} v_r \sin\theta d\theta. \quad (19)$$

Here θ is the emission angle of the fast moving atoms with respect to the symmetry axis, $\tan\theta_0=a/l$, σ_6 is the knock-out cross section and $v_r=(\bar{v}^2+v_c^2-2v_c\bar{v}\cos\theta)^{1/2} \simeq \bar{v}$ is the relative velocity of the colliding atoms [29]. Using the substitution $dl=v_c dt$ we can solve the differential equation under the boundary condition $\Phi(l)=\Phi_c$ at l=0 and obtain

$$\Phi(L) \simeq \Phi_c \exp\left[-\frac{1}{2}\sigma_6 n_s(\bar{v}/v_c)\int_0^L (1-\cos\theta_0)dl\right], \quad (20)$$

where $\cos\theta_0 = l/(l^2+a^2)^{1/2}$. In this model the density in the oven is taken to be uniform. Because for $l \gg a$ the collision probability vanishes we may freely extend the integral to infinity, $\int_0^\infty (1-\cos\theta_0)dl = a$. Hence, at the entrance of the 2D MOT the attenuated flux is given by

$$\Phi_{in} = \lim_{L\to\infty} \Phi(L) \simeq \Phi_c \exp(-\sigma_6 n_s \bar{v} \tau_6), \tag{21}$$

where $\tau_6 = a/2v_c \approx 47$ μs is the characteristic duration of the attenuation process.

To estimate σ_6 we take the approach of Ref. [37] and consider a slow atom moving at the capture velocity v_c along the symmetry axis from the oven toward the capture region. Fast atoms flying by with the thermal velocity $\bar{v}$ will give rise to momentum transfer as a result of van der Waals interaction. As this happens most frequently close to the oven even a small momentum transfer $\Delta p \lesssim 0.1\ mv_c$ suffices to kick the atoms out of the capture cone Ω_c. Because $\bar{v} \gg v_c$ the trajectory of the fast atom is hardly affected and the momentum transfer to the cold atom can be calculated by integrating the transverse component of the van der Waals force over time, $\Delta p = \frac{1}{2}\int_{-\infty}^{\infty} F_\perp(t)dt$. Here $F(r) = 6C_6/r^7$ with r the radial distance between the colliding atoms and $C_6 = 1389 a_0^6 E_h$ the van der Waals coefficient [38] with $a_0 \approx 0.529 \times 10^{-10}$ m the Bohr radius and $E_h \approx 4.36 \times 10^{-18}$ J the Hartree energy. Changing from the time variable t to the angular variable θ using $\tan\theta = \bar{v}t/b$, where b is the distance of closest approach, we obtain using $F_\perp = F\cos\theta$ and $\cos\theta = b/r$,

$$\Delta p = \frac{6C_c}{2\bar{v}b^6}\int_{-\pi/2}^{\pi/2} \cos^6\theta d\theta = \frac{C_6}{\bar{v}b^6}\frac{15\pi}{16}. \tag{22}$$

The critical distance of closest approach for which the atoms are just scattered outside the capture cone Ω_c is given by

$$b_6 \simeq 1.8(C_6/mv_c\bar{v})^{1/6}. \tag{23}$$

Note that this quantity depends only very weakly on the precise values of v_c and $\bar{v}$. For $v_c \approx 85$ m/s and temperatures in the range $600 \lesssim T \lesssim 700$ K we calculate for the knock-out cross section $\sigma_6 = \pi b_6^2 \approx 4.4 \times 10^{-14}$ cm^2. Note that, in contrast to "knock-out" collisions, "knock-in" collisions are rare. The steep dependence of Δp on b implies that most of the atoms scattered outside the acceptance cone scatter over much larger angles than the minimum angle required for knock out. Thus scattered atoms typically hit the wall of the oven tube and stick, rather than giving rise to knock in.

Along the same lines we estimate the momentum transfer by resonant collisions inside the 2D MOT. As the relative velocities are large and the typical collision time is much shorter than the lifetime of the atoms in the excited state we may use again the classical scattering model discussed above. In the present case the critical distance of closest approach corresponds to momentum transfer just exceeding the escape value from the 2D MOT, $mv \gtrsim mv_{esc}$ [37]. Neglecting the direction of the transition dipole the resonant-dipole force can be approximated by $F(r) = 3C_3/r^4$, where the C_3 coefficient is defined as [40,39]

$$C_3 = e^2 a_0^2 D_{eg}^2/4\pi\varepsilon_0 = 3.7 \times 10^{-48}\ \text{J m}^3. \tag{24}$$

Here $e \approx 1.60 \times 10^{-19}$ C is the elementary charge, $\varepsilon_0 \approx 8.85 \times 10^{-12}$ Fm^{-1} the electric constant and $D_{eg} = 2.4$ a.u. the transition dipole moment for the $2s \to 2p$ transition in Li [2]. The corresponding critical distance of closest approach is in this case

$$b_3 \simeq 1.6(C_3/mv_{esc}\bar{v})^{1/3}. \tag{25}$$

To obtain an order of magnitude estimate for b_3 we assume the escape velocity to be of the same order as the capture velocity, $v_{esc} = v_c$. For $v_c \approx 85$ m/s and temperatures in the range $600 \lesssim T \lesssim 700$ K we calculate for the resonant cross section $\sigma_3 = \pi b_3^2 \approx 1.6 \times 10^{-13}$ cm^2. Accounting for the knock-out probability of trapped atoms the loading rate into the 3D MOT can be written as

$$\Phi_r = \bar{\chi}_t \Phi_{in} \exp[-\sigma_3 \tau_{\text{res}} \Phi_s / A_c]. \tag{26}$$

Combining Eqs. (3) and (4) with the C_6 and C_3 loss exponents of Eqs. (21) and (26) and introducing the characteristic attenuation time $\tau_3 = A\tau_{\text{res}}/4\pi L^2$ we obtain the following expression for the 3D MOT loading rate:

$$\Phi_r \simeq \bar{\chi}_t a_6 n_s \bar{v} A \left(\frac{v_c}{\alpha}\right)^4 \frac{\Omega_c}{8\pi} \exp[-n_s\bar{v}(\sigma_6\tau_6 + \sigma_3\tau_3)], \tag{27}$$

Using $\tau_{\text{res}} = 1$ ms we have $\tau_3 \approx 1.6$ μs. Note that only α, $\bar{v}$, and n_s are sensitive for the oven temperature. A best fit of Eq. (27) to the data using $\bar{\chi}_t$ and n_s (at $T = 623$ K) as free parameters is shown as the solid line in Fig. 8. The fit shown is obtained for $\bar{\chi}_t = 0.33$ and $n_s = 1.5 \times 10^{17}$ m^{-3} at $T = 623$ K, which are both within the error limits given for these quantities. Thus also the position of the maximum confirms our model. As the result obtained for $\bar{\chi}_t$ strongly anticorrelates with the value presumed for v_c we cannot improve upon the estimate $\chi_{\max} = 30 \pm 10\%$ already given in Sec. V A.

Interestingly, comparing the two loss mechanisms we find $\sigma_3\tau_3/\sigma_6\tau_6 \approx 0.1$, which shows that the resonance mechanism, dominating the background losses in the VCMOT [22,37], is of minor importance in the present case. Since the output flux scales like $(v_c/\alpha)^4$ an obvious way to increase the output of MOT sources is to increase the capture velocity. Doubling the waist of the 2D MOT beams in the xy plane (see Fig. 1) in order to increase the capture radius we find with Eq. (9) that the capture velocity increases by $\sqrt{2}$ and the output by a factor 4. In addition, since τ_6 scales like $1/v_c$ the beam attenuation decreases slightly.

C. Comparison with Zeeman slowers

In several respects the 2D MOT source demonstrated in this paper represents an interesting alternative for the Zeeman slower. First of all the source yields a large controllable output flux of up to 3×10^9 s^{-1}, comparable to fluxes typically achieved in lithium Zeeman slowers. The transverse temperature of the source is low (1.4 mK) which makes it possible to recapture as much as 30% in a 3D MOT 220 mm downstream from the source. In contrast to Zeeman slowers, the 2D MOT source yields a clean and monochromatic cold atomic beam of which the most-probable velocity can be varied over a wide range of velocities with the aid of a push beam. Permanent magnets for the creation of the quadrupole field add to the simplicity of the design. The resulting source is more compact than a typical Zeeman slower and is still capable of loading 10^{10} atoms in a 3D MOT.

Importantly, the 2D MOT principle works equally well with light atoms as with more heavy atoms like K, Rb, and

Cs. This shows that, like the Zeeman slower, also the 2D MOT beam source has a wide applicability. In cases with a sizable vapor pressure at room temperature the source will act as a VCMOT. As an example of a system for which a 2D MOT as a source has not yet been realized we briefly discuss the case of Na [41]. In this case the gradient of the quadrupole field should be scaled down proportional to $m^{1/2}$ in accordance with Eq. (8) to obtain the optimum value $\partial B/\partial r \approx 0.25$ T/m. In view of Eq. (9) the capture velocity scales down with the same factor. Using Eq. (27) we calculate for Na a maximum total output flux of 4×10^9 s^{-1} for an oven temperature $T\approx471$ K. This output is lower than realized with Zeeman slowers but the oven is operated at much lower temperature [12–14].

Unlike the output of the Zeeman slower the output of the 2D MOT source is limited by a fundamental loss mechanism. As described in Sec. V B this is caused by van der Waals forces between atoms leaving the oven and (to a lesser extent) by resonant-dipole forces between optically excited atoms in the 2D MOT and the hot background flux from the oven. These losses are quantified by the exponent in Eq. (27), which is shown as the dashed line in Fig. 8. Note that near maximum output at $T\approx700$ K the attenuation factor is already as small as ~0.3. Therefore, the source is best operated at temperatures below 650 K, where the flux may be slightly smaller but the depletion time of the oven is comfortably long. Alternatively, one could incorporate a recycling principle [11,15].

VI. SUMMARY AND CONCLUSION

We developed a beam source for cold ^{6}Li atoms. The source is based on the 2D MOT principle and yields a controllable output flux of up to 3×10^9 s^{-1}, comparable to fluxes typically achieved in lithium Zeeman slowers. Some 30% of the atoms are recaptured into a 3D MOT 220 mm downstream from the source. The source is side loaded from an oven and a push beam assures that only capturable atoms enter the main vacuum chamber. This yields a clean and quite monochromatic cold atomic beam of which the most-probable axial velocity α_z can be varied over the range $18 \lesssim \alpha_z \lesssim 70$ m/s by varying the intensity of the push beam. The 2D MOT can be fully optimized for capture because the push beam assures that the density of trapped atoms is intrinsically low. The push beam also drastically simplifies the alignment of the 2D MOT. Permanent magnets simplify the implementation of the quadrupole field. The resulting source is compact and enables us to load up to 10^{10} atoms into a 3D MOT, which is sufficient as a starting point for most experiments with quantum gases. The output flux increases exponentially with the oven temperature until at $T\approx700$ K a loss mechanism limits the flux. We identify knock-out collisions near the oven exit as a result of van der Waals forces between the atoms as the limiting mechanism. At maximum output the beam attenuation factor is ~0.35. Therefore, the source is more efficiently operated at a lower oven temperature. For $T=623$ K we measured a loading rate of $\Phi_r = 1.8(6)\times10^8$ s^{-1} in the 3D MOT. At this temperature the uninterrupted running time on 8 g of lithium is $\sim17\,000$ h. With our work we demonstrate that the 2D MOT principle works equally well with light atoms as with more heavy atoms and is likely to be suitable for any atomic system with an optical cooling transition.

ACKNOWLEDGMENTS

The authors thank P. Cleary and M. Koot for assistance with the characterization of the $Nd_2Fe_{14}B$ magnets, G.V. Shlyapnikov and T.W. Hijmans for stimulating discussions and N. J. van Druten for critically reading the paper. This work is part of the research program on Quantum Gases of the Stichting voor Fundamenteel Onderzoek der Materie (FOM), which is financially supported by the Nederlandse Organisatie voor Wetenschappelijk Onderzoek (NWO).

[1] W. D. Phillips and H. J. Metcalf, Phys. Rev. Lett. **48**, 596 (1982).
[2] H. J. Metcalf and P. van der Straten, *Laser Cooling and Trapping* (Springer, New York, 1999).
[3] I. F. Silvera and J. T. M. Walraven, Phys. Rev. Lett. **44**, 164 (1980).
[4] J. D. Weinstein, R. deCarvalho, T. Guillet, B. Friedrich, and J. M. Doyle, Nature (London) **395**, 148 (1998).
[5] B. Ghaffari, J. M. Gerton, W. I. McAlexander, K. E. Strecker, D. M. Homan, and R. G. Hulet, Phys. Rev. A **60**, 3878 (1999).
[6] E. Nikitin, E. Dashevskaya, J. Alnis, M. Auzinsh, E. R. I. Abraham, B. R. Furneaux, M. Keil, C. McRaven, N. Shafer-Ray, and R. Waskowsky, Phys. Rev. A **68**, 023403 (2003).
[7] S. A. Rangwala, T. Junglen, T. Rieger, P. W. H. Pinkse, and G. Rempe, Phys. Rev. A **67**, 043406 (2003).
[8] H. L. Bethlem, G. Berden, and G. Meijer, Phys. Rev. Lett. **83**, 1558 (1999).
[9] E. Vliegen and F. Merkt, J. Phys. B **39**, L241 (2006).
[10] F. Lison, P. Schuh, D. Haubrich, and D. Meschede, Phys. Rev. A **61**, 013405 (1999).
[11] C. Slowe, L. Vernac, and L. V. Hau, Rev. Sci. Instrum. **76**, 103101 (2005).
[12] C. A. Stan and W. Ketterle, Rev. Sci. Instrum. **76**, 063113 (2005).
[13] M. A. Joffe, W. Ketterle, A. Martin, and D. E. Pritchard, J. Opt. Soc. Am. B **10**, 2257 (1993).
[14] K. M. R. van der Stam, E. D. van Ooijen, R. Meppelink, J. M. Vogels, and P. van der Straten, Rev. Sci. Instrum. **78**, 013102 (2007).
[15] See, e.g., L. Vestergaard Hau, J. A. Golovchenko, and M. M. Burns, Rev. Sci. Instrum. **65**, 3746 (1994).
[16] C. Monroe, W. Swann, H. Robinson, and C. Wieman, Phys. Rev. Lett. **65**, 1571 (1990).
[17] K. L. Moore, T. P. Purdy, K. W. Murch, S. Leslie, S. Gupta, and D. M. Stamper-Kurn, Rev. Sci. Instrum. **76**, 023106 (2005).

[18] A. Gozzini, F. Mango, J. H. Xu, G. Alzetta, F. Maccarone, and R. A. Bernheim, Nuovo Cimento D **15**, 709 (1993).
[19] C. Klempt, T. van Zoest, T. Henninger, O. Topic, E. Rasel, W. Ertmer, and J. Arlt, Phys. Rev. A **73**, 013410 (2006).
[20] C. J. Myatt, N. R. Newbury, R. W. Ghrist, S. Loutzenhiser, and C. E. Wieman, Opt. Lett. **21**, 290 (1996).
[21] Z. T. Lu, K. L. Corwin, M. J. Renn, M. H. Anderson, E. A. Cornell, and C. E. Wieman, Phys. Rev. Lett. **77**, 3331 (1996).
[22] K. Dieckmann, R. J. C. Spreeuw, M. Weidemüller, and J. T. M. Walraven, Phys. Rev. A **58**, 3891 (1998).
[23] J. Schoser, A. Batär, R. Löw, V. Schweikhard, A. Grabowski, Yu. B. Ovchinnikov, and T. Pfau, Phys. Rev. A **66**, 023410 (2002).
[24] J. Catani, P. Maioli, L. De Sarlo, F. Minardi, and M. Inguscio, Phys. Rev. A **73**, 033415 (2006).
[25] C. B. Alcock, V. P. Itkin, and M. K. Horrigan, Can. Metall. Q. **23**, 309 (1984).
[26] Y. Fukuyama, H. Kanou, V. I. Balykin, and K. Shimizu, Appl. Phys. B: Lasers Opt. **70**, 561 (2000).
[27] K. Honda, Y. Takahashi, T. Kuwamoto, M. Fujimoto, K. Toyoda, K. Ishikawa, and T. Yabuzaki, Phys. Rev. A **59**, R934 (1999).
[28] A. Griesmaier, J. Werner, S. Hensler, J. Stuhler, and T. Pfau, Phys. Rev. Lett. **94**, 160401 (2005).
[29] I. Estermann, O. C. Simpson, and O. Stern, Phys. Rev. **71**, 238 (1947).
[30] J. Vanier and C. Audoin, *The Quantum Physics of Atomic Frequency Standards* (Adam Hilger, Bristol, 1989).
[31] K. Ladouceur, B. G. Klappauf, J. van Dongen, N. Rauhut, B. Schuster, A. K. Mills, D. J. Jones, and K. W. Madison, J. Opt. Soc. Am. B **26**, 210 (2009).
[32] D. Das and V. Natarajan, Phys. Rev. A **75**, 052508 (2007).
[33] U. Schünemann, H. Engler, M. Zielonkowski, M. Weidemüller, and R. Grimm, Opt. Commun. **158**, 263 (1998).
[34] L. Ricci, M. Weidemüller, T. Esslinger, A. Hemmerich, C. Zimmermann, V. Vuletic, W. König, and T. W. Hänsch, Opt. Commun. **117**, 541 (1995).
[35] J. R. Vidal and J. Cooper, J. Appl. Phys. **40**, 3370 (1969).
[36] J. Kawanaka, K. Shimizu, and H. Takuma, Appl. Phys. B: Photophys. Laser Chem. **57**, 113 (1993).
[37] A. M. Steane, M. Chowdhury, and C. J. Foot, J. Opt. Soc. Am. B **9**, 2142 (1992).
[38] A. Derevianko, J. F. Babb, and A. Dalgarno, Phys. Rev. A **63**, 052704 (2001).
[39] P. R. Fontana, Phys. Rev. **123**, 1871 (1961).
[40] H. Margenau and N. R. Kestner, *Theory of Intermolecular Forces* (Pergamon Press, Oxford, 1971).
[41] E. Riis, D. S. Weiss, K. A. Moler, and S. Chu [Phys. Rev. Lett. **64**, 1658 (1990)] have presented an atom funnel for Na. This method is similar to the presented 2D MOT geometry, but with the addition of a slowing beam opposing the hot flux and axial cooling beams.